Available online at www.sciencedirect.com
SCIENCE DIRECT®
Nuclear Instruments and Methods in Physics Research A 498 (2003) 190–210
NUCLEAR INSTRUMENTS & METHODS IN PHYSICS RESEARCH Section A
www.elsevier.com/locate/nima

The DRAGON facility for nuclear astrophysics at TRIUMF-ISAC: design, construction and operation

D.A. Hutcheon[a], S. Bishop[b], L. Buchmann[a], M.L. Chatterjee[c], A.A. Chen[b,1], J.M. D'Auria[b,*], S. Engel[d], D. Gigliotti[e], U. Greife[f], D. Hunter[b], A. Hussein[e], C.C. Jewett[f], N. Khan[a], M. Lamey[b], A.M. Laird[a], W. Liu[b], A. Olin[a,g], D. Ottewell[a], J.G. Rogers[a], G. Roy[h], H. Sprenger[a], C. Wrede[b]

[a] *TRIUMF, Vancouver, BC, Canada*
[b] *Chemistry Department, Simon Fraser University, 8888 University Drive, Burnaby, BC, Canada*
[c] *Saha Institute of Nuclear Physics, Calcutta, India*
[d] *Ruhr-Universität, Bochum, Germany*
[e] *University of Northern British Columbia, Prince George, BC, Canada*
[f] *Colorado School of Mines, Golden, CO, USA*
[g] *University of Victoria, Victoria, BC, Canada*
[h] *University of Alberta, Edmonton, Alta., Canada*

Received 11 October 2002; accepted 7 November 2002

Abstract

A facility for measuring cross-sections (resonance strengths) for reactions of astrophysical importance involving short-lived, radioactive reactants has been designed, built and installed at the new TRIUMF-ISAC Radioactive Beams Laboratory in Canada. Named DRAGON (Detector of Recoils And Gamma-rays of Nuclear reactions), it has been successfully commissioned with stable and radioactive heavy ion beams from ISAC. This report presents the main components of the facility, namely, the windowless gas target, the surrounding γ detector array, the subsequent electromagnetic recoil mass separator, the focal plane detectors for recoils, the detection system for elastics, and the modular electronics and computer software used for the data acquisition. Examples of the operation of the facility for both stable beam reactions and the first radioactive beam reaction study, $^{21}Na(p,\gamma)^{22}Mg$ are also presented, along with future plans for the program.

PACS: 29.0

Keywords: Recoil mass separator; Nuclear reactions; Electric and magnetic devices; γ detector array; Windowless gas target system; Detectors

1. Introduction

DRAGON (Detector of Recoils And Gamma-rays Of Nuclear reactions) is TRIUMF's new

*Corresponding author. Tel.: +1-604-291-4607; fax: +1-604-291-3765.
E-mail addresses: dauria@sfu.ca (J.M. D'Auria), rogers@triumf.ca (J.G. Rogers).
[1] Present address: McMaster University, Hamilton, Canada.

0168-9002/03/$ - see front matter
doi:10.1016/S0168-9002(02)01990-3

facility for measuring radiative capture cross sections of astrophysical interest. DRAGON uses the accelerated radioactive beams produced at the ISAC (Isotope Separator and ACelerator) facility to measure cross sections in inverse-reaction kinematics. Reported herein are the design features of DRAGON as well as results of commissioning measurements with stable beams of ^{16}O, ^{15}N, and ^{20,21}Ne on a hydrogen gas target. The first astrophysics experiment utilized a ^{21}Na radioactive beam on the same hydrogen target. In the future a wide variety of radioactive beams will be used with hydrogen and helium gaseous targets.

Radiative capture reactions are believed to be important steps for many nucleosynthesis pathways and energy generation in a variety of stellar scenarios. Radiative capture of a radioactive nucleus with hydrogen or helium is important in that it provides a mechanism for extending the step-by-step nucleosynthesis of light elements to the production of heavy elements in explosive scenarios such as novae and X-ray bursts. For example, helium capture by radioactive ^{15}O may provide the only breakout path from the hot CNO cycle, which would otherwise end with the production of oxygen. The relative rate of radiative capture vs. the rate of the competing β decay determines the rate of nucleosynthesis for all isotopes in the reaction chain beyond the mass of the breakout nucleus.

Since the Coulomb barrier between the capture nucleus and hydrogen/helium keeps the reactants far apart even at typical explosive stellar temperatures, the important radiative capture cross sections are small compared to other processes at the same energies, such as elastic scattering. Laboratory measurement of such small cross sections is difficult, and requires design of the special detection apparatus to be described. Even so, measuring the smallest cross sections, such as $^{15}O(\alpha,\gamma)^{19}Ne$, may require weeks or months of radioactive beam time at TRIUMF-ISAC.

Following the capture reaction of the heavy beam particle with a hydrogen or helium nucleus, the final state consists of one or more γ-rays, typically of energies 1–10 MeV, and a heavy-ion recoiling in the forward direction. Since the γ-rays carry very little momentum compared to the heavy-ion, inverse kinematics restrict the heavy-ion to a narrow forward cone, nearly parallel to the beam while the γ-ray(s) are emitted into a wider sphere.

1.1. The facility: general

DRAGON is located in the ISAC hall at TRIUMF on the high energy beam line [1]. ISAC delivers isotopically pure radioactive heavy-ion beams as well as stable beams from an off-line ion source (OLIS) with energies between 0.15 and 1.5 MeV/u. DRAGON (Fig. 1) consists of four main components, namely, a windowless, recirculating gas target, a γ-detector array, an electromagnetic separator (EMS), and a heavy-ion recoil detection system. This article describes these hardware components, associated electronics and software, and presents commissioning data acquired to validate desired functioning of the

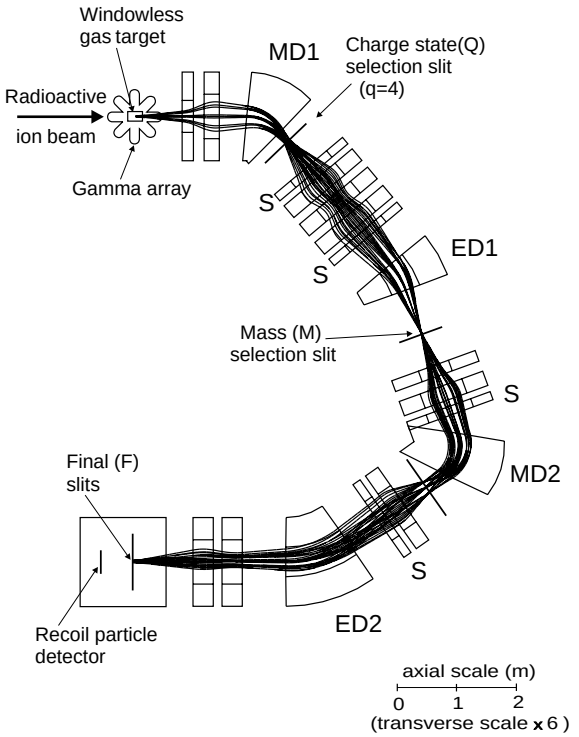

Fig. 1. Schematic representation of the DRAGON layout with typical ion trajectories. The transverse scale has been magnified 5X to display apertures and ion trajectories.

facility. Here follows a brief description of each part of DRAGON, to be expanded on in later sections.

The heavy ion beam enters the target gas cell (Fig. 2) through a series of differentially pumped tubes. The gas pressure in the cell is regulated to be in the range from 0.2 to 10 Torr, and the gas density is uniform over most of the 11 cm between the innermost apertures. The downstream gas pressure is reduced by differential pumping through a second set of tubes until it reaches 10^{-6} Torr at the entrance to the first magnetic element of the separator, 1 m downstream of the target cell. The gas target cell also contains a solid-state detector which measures the rate of elastic scattering by detecting hydrogen or helium recoil ions.

The γ-detector array is comprised of 30 BGO (Bismuth Germanate) scintillation crystals of hexagonal cross section (Fig. 3) which are stacked in a close-packed array surrounding the gas target (Fig. 4). Monte Carlo simulations [2] predict that the γ-ray detection efficiency of the array varies from 45% to 60% for 1–10 MeV γ-rays over the 11 cm target length. Confirmation of these simulations by efficiency measurements are in progress using standard γ sources [3]. Among the 30 detectors the γ energy resolution at 6.13 MeV averages 7% full-width half-maximum (FWHM).

The heavy-ion recoil leaves the target parallel to the beam and DRAGON accepts recoils within

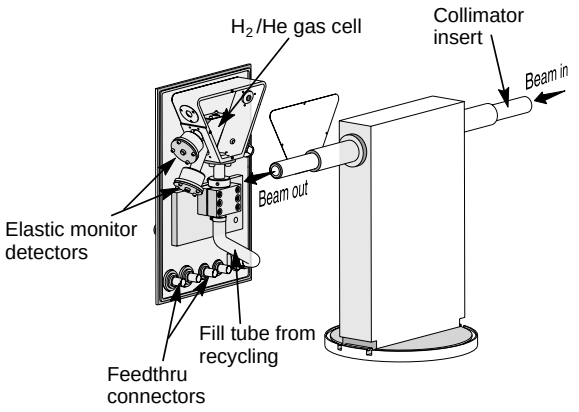

Fig. 2. Schematic representation of the inner components of the DRAGON windowless gas target system.

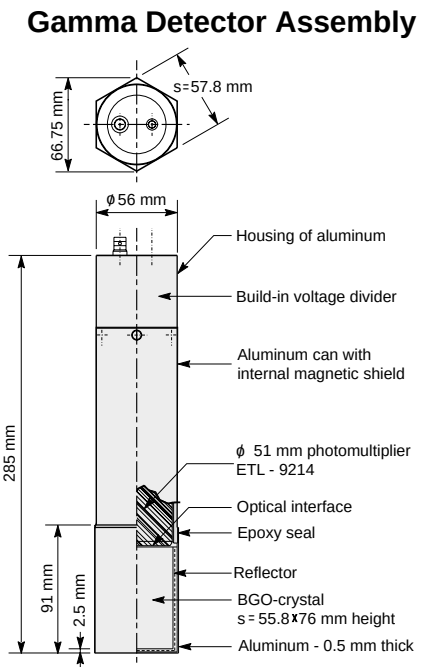

Fig. 3. One of the γ-ray scintillation detector composed of a BGO crystal coupled to a 51 mm diameter photomultiplier tube.

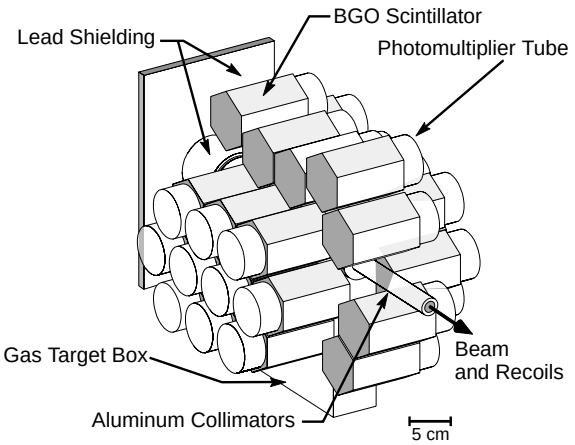

Fig. 4. The DRAGON BGO γ array, composed of 30 BGO units, surrounding the gas target region.

± 20 mrad or less. The smaller the γ-ray energy, the closer the recoil trajectory follows the beam direction. The maximum recoil opening angle varies from reaction to reaction, depending on the masses and Q-values of the capture reaction

Table 1
Parameters of radiative reactions in the DRAGON program

Reaction	E_x (MeV)	E_{beam} (MeV/u)	E_{recoil} (MeV/u)	E_γ (MeV)	Recoil cone (mrad)	Required suppression
$^{13}N(p,\gamma)^{14}O(DC)$	4.8–6.2	0.1–0.6		5		10^{-8}–10^{-13}
$^{15}O(\alpha,\gamma)^{19}Ne$	4.033	0.16	0.10	4.03	15.6	10^{-15}
$^{17}F(p,\gamma)^{18}Ne$	4.561	0.68	0.60		7.6	10^{-11}
$^{18}F(p,\gamma)^{19}Ne$	6.742	0.35	0.31		14.7	10^{-11}
	6.862	0.48	0.43		12.8	10^{-11}
$^{19}Ne(p,\gamma)^{20}Na$	2.646	0.47	0.42	2.2	4.7	10^{-11}
$^{20}Na(p,\gamma)^{21}Mg$	3.508	0.31	0.28		7.3	10^{-9}
$^{21}Na(p,\gamma)^{22}Mg$	5.714	0.22	0.20	5.5	13.3	5×10^{-12}
$^{23}Mg(p,\gamma)^{24}Al$	2.38	0.53	0.49	1.87	3.30	10^{-10}
$^{25}Al(p,\gamma)^{26}Si$	5.97	0.47	0.44		8.1	
$^{26m}Al(p,\gamma)^{27}Si$	7.893	0.23	0.21		15.0	

being studied (Table 1). The DRAGON EMS (Fig. 1) is designed to accept recoils and separate them from beam particles for relevant reactions attainable with ISAC's radioactive beams. The separator consists of a series of magnetic dipoles (M), magnetic quadrupoles (Q) magnetic sextupoles (S) and electrostatic dipoles (E). Arranged in the order (QQMSQQQSE)(QQSMQSEQQ), they form two stages of mass separation. After being bent away from the recoils, the separated beam is stopped on slits between the electromagnetic elements. The recoils of a selected charge state (most probable state $\geqslant 40\%$) are transmitted with an efficiency of approximately 100% to the focal plane detection systems. In studies reported herein, a double-sided silicon-strip detector (DSSSD) oriented perpendicular to the heavy-ion's trajectory was employed. The DSSSD measures recoil energy and two-dimensional position over a 5×5 cm^2 area. Future detection systems for use at the final focus include a microchannel plate detection system for fast timing and a thin window ionization chamber. The length of the separator from gas target to recoil detector is 21 m.

The detectors described above are interfaced to NIM electronics modules, which are in-turn interfaced to a TRIUMF-standard data acquisition computer via CAMAC. The hardware and software are configured to simultaneously acquire events from all detectors operated in singles-mode, and at the same time coincidence-events corresponding to the detection of heavy-ion recoils in delayed coincidence with one or more γ-rays. The heavy-ion's time-of-flight is typically 1–4 μs over the 21 m distance between γ array and heavy-ion detector. Imposing a tight time-of-flight requirement between the gamma and the recoil detectors has proven to be a powerful tool to reduce background.

2. Windowless gas target

The radiative capture reactions of interest in astrophysics are characterized by narrow energy widths, typically less than the 1 keV/u (FWHM) energy spread of the available ISAC beams. In addition, the resonant energy is often only known to a few percent. Thus it is a challenge to select the correct beam energy so that given the energy loss in the target, the resonant reaction occurs inside the target cell where the detectors are focused. This condition implies the need for a thick target, meaning that the energy loss from front to back in the target should be substantially more than the typical ISAC beam energy widths and the uncertainty in the resonance energy.

The target was designed for 4.5 Torr (although it has operated up to 8 Torr) of gas pressure and 11 cm of length. The selected pressure and length represented a compromise between the required pumping capacity on the one hand and the need for a simple EMS design on the other. If the chosen gas pressure were too high, the pumps to

recirculate the gas leaking out of the beam apertures would be too expensive. If the target length were too long the apparent beam spot size would increase, making it harder to separate beam from recoils in the EMS. The required beam–recoil separation in the EMS, characterized by a "suppression factor", is discussed in greater detail below.

The gas cell is contained in a rectangular pumping box, shown partially cut away in Fig. 2. The design of the cell and box represents another compromise, between the need to detect γ-rays efficiently with a compact array and the need for good pumping in regions adjacent to the cell. The gas supply line plus feed-throughs for a beam intensity monitor, pressure transducer and thermocouple all pass through the lower part of a removable side plate of the tall, narrow box. The gas cell mount also attaches to the lower part of this plate. The box is made of aluminum, as thin as possible to reduce the mass of extraneous absorber between source and the γ detectors. This design allows the γ detection array to subtend about 80% of the (4π) solid angle, viewing from the center of the target, and gives a high γ detection efficiency, as mentioned earlier.

It is especially important to obtain good vacuum ($<10^{-6}$ Torr) downstream of the target because charge changing reactions (see discussion below) of beam particles in residual gas could potentially degrade the suppression factor of the EMS.

The gas cell has a beam entrance aperture of 6 mm and an exit aperture of 8 mm diameter due to the expected beam size and recoil divergence angle. The ends of the cell are slanted at 30° with respect to the vertical, so that the jets of gas coming out of the cell are directed downward away from the entrance to the tubes of the differential pumping system. Use of the inclined apertures demonstrated a factor-of-3 reduction in pressure at the end of the differential pumping stages for hydrogen gas, compared to the original design with vertical ends.

The bottom of the box is connected by a 15-cm diameter pipe to large Roots blowers (two Leybold WSU2001, two WSU501, one WS500), the first stage of differential pumping (Fig. 5). The three stages of blower compression raise pressures to >

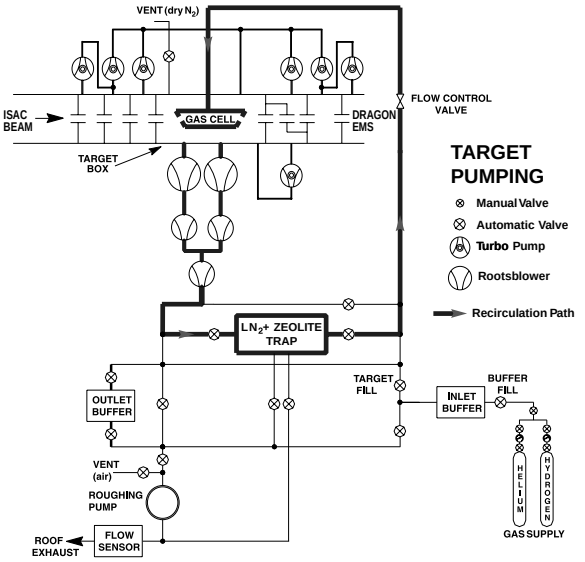

Fig. 5. Schematic representation of the DRAGON windowless gas target and recirculation system.

40 Torr at the inlet to a 20-l cleaning trap, allowing gas to dwell in the trap for times of order 10 s. The trap contains 2 l of X-13 (Zeolite) molecular sieve at liquid nitrogen temperature. The molecular sieve adsorbs approximately 50 atm l of hydrogen when the trap pressure is brought up to 45 Torr. This inventory of stored hydrogen contributes to the operational stability of the target; cell pressures routinely are steady to better than 1% with no adjustment of the flow control valve.

A series of pumping tubes connect pumping boxes to which are attached 1000 l/s turbomolecular pumps (Varian V1000HT), as shown in Fig. 5. The inner surfaces of the pumping tubes, as shown in Fig. 6, are stepped or tapered to conform to the expected beam convergence and the cone angle of the outgoing recoils (5 mrad half-angle upstream, 20 mrad half-angle downstream). Three upstream turbo pumps and four downstream turbo pumps achieve pressures of $<3\times10^{-6}$ Torr at the ends of the pumping system for a hydrogen gas pressure of 4.5 Torr in the inner target cell, a level that is compatible with the design pressure and available pumping in the EMS. Apertures and pumping tubes are

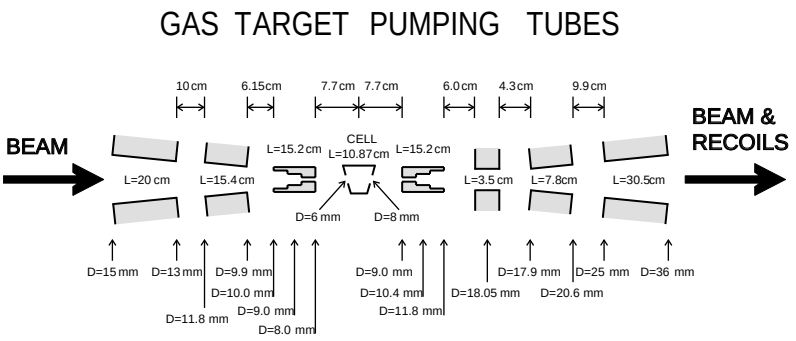

Fig. 6. Details of the apertures of the DRAGON gas target system.

removable and can be changed to other sizes to accommodate actual beam- and recoil-cones encountered in various experimental situations.

2.1. Commissioning the gas target

Initial studies using the gas target were performed to determine charge state distributions resulting from the interaction of low energy heavy ions passing through the gas; results of these are reported elsewhere [1,4].

Measurements to study the operation and pressure profile of the gas target (with hydrogen) were performed with a variable energy ^{15}N beam. The emission rate of 4.4 MeV secondary γ-rays from a narrow resonance at 420 keV/u in the ^{15}N(p, $\alpha\gamma$)^{12}C reaction [5] were recorded in a γ array configured to give uniform efficiency over 20 cm along the beam line.

The resulting excitation function is shown in Fig. 7 for two different target gas pressures. As the beam energy increases, the rate of γ emission increases sharply at the energy of 425 keV/u, i.e. when the resonant energy occurs near the upstream aperture of the target. It then remains constant as the energy increases further, up to the energy when the resonance occurs near the downstream aperture of the target. At this energy the γ yield falls sharply to a background level about a factor-of-300 lower than the value it had when the resonance was contained in the target cell between the apertures. The maximum yield is independent of the target gas pressure, as expected.

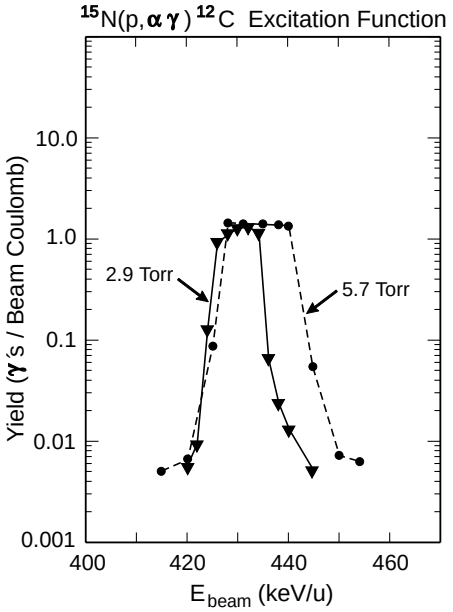

Fig. 7. Excitation function for the ^{15}N(^{1}H, $\alpha\gamma$)^{12}C reaction around the narrow resonance at a beam energy of 420 keV/u. The shape of the 4.4 MeV, γ-ray yield curve is characteristic of the thick target.

The effective length of the target is defined to be the distance between the γ-ray emission points where the yield falls to half its peak value. This length was determined by converting the energy-widths of the thick-target-yield curves (Fig. 7) to lengths, using the known energy loss of 0.221 keV/u/(Torr-cm) according to the SRIM code [6] for ^{15}N ions in hydrogen. This gave 12 cm effective target length for the 5.7 Torr data and 13 cm for the 2.9 Torr data.

A more accurate target length was determined by measuring the energy loss of beam ions through the target [7]. The 6 and 8 mm (diameter) collimators for the inner target cell were replaced with 1.5 mm collimators, so that less than 1% of the gas intercepted the beam outside the cell. For the same central pressure, the ratio of energy losses in the two collimator configurations is equal to the ratio of their effective lengths. With a ^{21}Ne beam at 275 keV/u, this ratio was measured to be 1.109, which translates into an effective target length of 12.3 ± 0.4 cm for the 6/8 mm collimation; the energy loss was 83 ± 2 eV/10^{15} atoms/cm^2.

These effective lengths are slightly larger than the 11 cm geometric length between the inner apertures. Some such extension of the effective length over the geometric length should be expected because the pressure outside the inner cell is not zero, but estimated at about 10% of the pressure inside. The γ array and EMS were designed to have uniform acceptance over a 10 cm range of reaction positions.

In measuring broad resonances, a significant part of the yield may come from radiative capture in the residual gas outside the gas cell apertures. To convert yield to cross sections for these reactions may require future measurement of the target gas density profile beyond the inner apertures. Section 9 covers other features in the study of broad resonances with DRAGON.

3. γ-detector array

The γ-detector array (Fig. 4) consists of 30 scintillation detectors in a close-packed configuration around the target. Monte Carlo simulation was used to optimize efficiency for detection of 1–10 MeV γ-rays originating from the 10 cm long gas target volume [2]. Two important criteria were given equal weight in designing the array: (1) It must count fast to reject the background from stray radioactive beam particles which stop in the target, emitting two 511 keV annihilation γ-rays. With the ^{21}Na beam this rate already reached one million counts/s in some detectors, and may go higher when more intense beams become available. (2) It must have the best possible energy resolution. To separate the capture γ-rays from the background, it is necessary to discriminate against low-energy γ-rays. Even though the background is caused by 511 keV γ-rays, they often pile-up and masquerade as higher-energy γ-rays [8].

BGO was selected for the scintillator after considering more exotic crystals such as BaF_2, GSO and LSO [9]. BGO has an advantage over these others in that it emits light with a simple exponential time-constant, i.e. without longer-time components or afterglow [10]. BGO also has the advantage of the highest density of any modern scintillator [11], which leads to good efficiency in a compact, and therefore economical, array. For BGO the maximum, i.e. worst, attenuation length in our energy range is 5 cm at 5 MeV [11]. To match the maximum attenuation length to an economical photomultiplier tube (PMT) we chose the detecting element to be a 76 mm long by 56 mm (hexagonal shaped cross-section) cylinder of BGO coupled to a 51 mm cylindrical PMT. This detector size required 30 units to fill the available solid-angle around the target (Fig. 4).

3.1. γ-detector quality assurance

The specified performance of individual BGO detectors in energy resolution and rate-handling capability were: (1) The energy resolution should be 12.5% FWHM or better at 667 keV and (2) the gain shift should be less than 1% for counting rates between 0 and 500 K counts/s. To minimize the rate effects we designed the PMT bases to have maximum dynode bias current by using the minimum dynode resistor values recommended for the selected PMTs.[2] Even so, the rate requirement proved difficult to satisfy and required several iterations between TRIUMF and the manufacturers.

3.2. γ-array calibration

Fig. 8 shows selected detectors' pulse-height spectra using a 6.13 MeV calibration source

[2] The gamma detector PMT's were Hamamatsu R1828-01 and Electron Tubes Ltd (ETL)9214. The base resistor values were 100 kΩ between dynodes 3 and 8 and then increased to a maximum of 300 kΩ between dynode-11 and dynode-12.

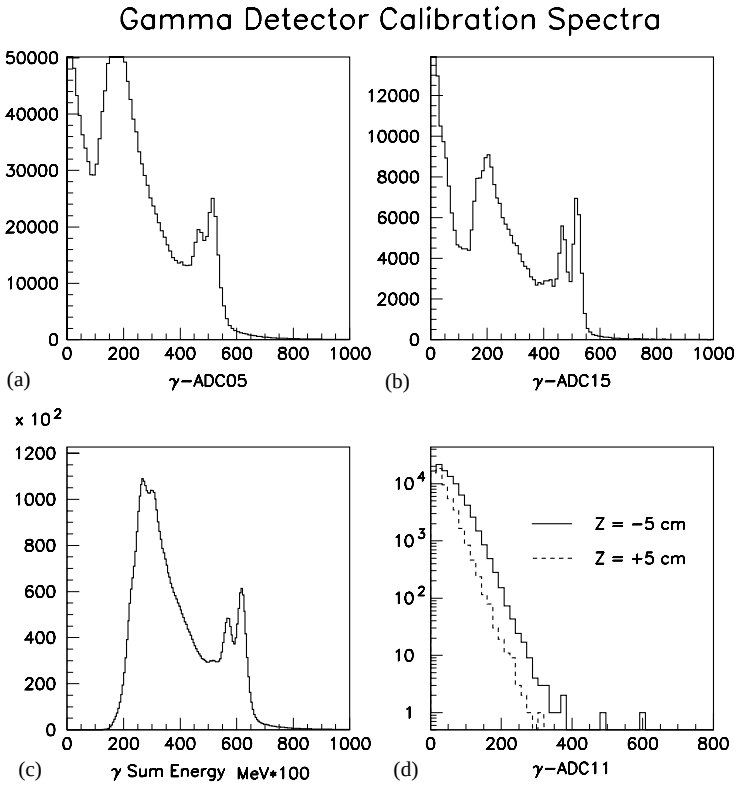

Fig. 8. (a) Pulse-height spectra using the BGO γ array with a 6.13 MeV γ-ray source for the poorest resolution detector, (b) for the best resolution detector, (c) the average resolution, and (d) for the 865 keV/u ^{21}Na beam spill spectrum in two typical detectors.

(^{244}Cm/^{13}C); Figs. 8a–c show the worst-, best-, and average-resolution of 9%, 6%, and 7%, respectively. This energy resolution is worse than the factory specification because of partial integration in the charge sensitive Analogue–Digital Converter (ADC), as discussed below (Section 7.1). Fig. 8d displays the pileup spectrum obtained with radioactive beam spill in two separate detectors located upstream (−5 cm) and downstream (+5 cm) of the target center.

4. Electromagnetic mass separator (EMS)

The kinematics of radiative capture reactions sets the specifications for the mass separator. For illustration, we consider the ^{21}Na(^{1}H, γ)^{22}Mg reaction. In the center-of-mass system the ^{22}Mg nucleus has a relatively low momentum (a few MeV/c) which is constrained to lie within a sphere whose radius is proportional to the total energy of the decay γ-ray(s). In inverse kinematics the center-of-mass recoil momenta are boosted forward, to lie within a small cone of lab angles around the beam direction, and recoil momenta in the laboratory system centered on the beam momentum. For this reaction, for example, the cone half-angle is 13 mrad and the energy spread of recoils is $\pm$2.6% of beam energy.

Beam and recoils emerge from the target in a range of charge states, the most populated state typically containing 35–50% of the particles [1]. The associated magnetic rigidities for most-populated charge states are not more than 0.5 T m for the beams that can be accelerated in ISAC-I.

Since beam and desired product emerge with almost the same momentum and the beam may have a low energy tail, both electrostatic and

magnetic elements are needed in the separator. We chose a design in which the first dipole is magnetic to allow selection of one of the charge states with which ions emerge from the gas target, followed by an electrostatic dipole. This avoids having beam ions in non-selected charge states striking smooth electrodes at glancing angles, which might happen if the first dipole is electrostatic. Quadrupoles bring the ions to an achromatic focus after the electrostatic dipole, where slits allow transmission of the desired recoil product while blocking the beam particles. A second stage with larger bend angles contains a magnetic dipole followed by an electrostatic dipole. A preliminary optics design had the second stage with electrostatic followed by magnetic bending, but simulations showed that this combination (M–E–E–M) could transmit beam particles which had two charge-changing collisions with residual gas. The final M–E–M–E combination requires three such charge changes.

As well as charge-changing collisions with residual gas, simulations considered a white spectrum of particles passing through the charge state selection slits at a variety of angles, as might arise if beam particles scattered off the pumping tubes of the gas target. It was verified that such particles could not pass through the final selection slits, if no further scattering from walls or residual gas took place.

The arrangement of focusing quadrupoles and aberration correcting sextupoles is shown in Fig. 1 along with the envelope of ion trajectories in the horizontal plane, for ions of different initial angles and energies. The ion optical calculations [12] was carried out to third order using the computer code GIOSP [13], and simulated using GEANT [14] and RAYTRACE [15] for the ^{19}Ne recoils resulting from the important $^{15}O(\alpha,\gamma)^{19}Ne$ reaction. In addition to the four sextupoles shown, a small sextupole component was built into quadrupole Q2 by shaping the pole tips. First order transfer matrix elements from the target to each of three focus locations are presented in Table 2. The mass resolution is modest ($M/\delta M = 600$ to first order, for a 3-mm beamspot at the target), in keeping with the beam–recoil differences of $M/\delta M = 15$–30 for the proton capture experiments. Considerable effort went into keeping calculated second-order aberrations smaller than the first-order contributions at the two achromatic focus locations.

Table 2
GIOS first-order transfer matrix elements at the four horizontal image points: x is horizontal position (m); a is horizontal angle (rad); y is vertical position (m); b is vertical angle (rad); d is fractional energy difference; g is fractional mass difference; t is fractional difference in time-of-flight

	Charge	Mass	Charge′	Final
$(x\|x)$	−0.440	0.689	−0.580	0.980
$(x\|a)$	0.000	0.000	0.000	0.000
$(x\|g)$	0.302	−0.472	1.081	−1.828
$(x\|d)$	0.302	0.000	0.684	0.000
$(a\|x)$	−1.648	1.147	−2.122	0.052
$(a\|a)$	−2.273	1.451	−1.725	1.020
$(a\|g)$	0.401	−0.321	1.589	1.303
$(a\|d)$	0.401	0.015	0.669	−0.022
$(t\|x)$	0.172	0.002	0.161	−0.002
$(t\|a)$	0.368	0.000	0.179	0.000
$(t\|g)$	0.515	0.504	0.462	0.515
$(t\|d)$	−0.485	−0.492	−0.482	−0.477
$(y\|y)$	−3.554	0.980	3.487	−1.767
$(y\|b)$	0.018	−0.430	0.227	0.000
$(b\|y)$	−1.563	2.307	−3.336	1.657
$(b\|b)$	−0.273	0.008	0.070	−0.566

Table 3
Properties of DRAGON magnetic dipoles

	MD1	MD2
Bending radius	1.00 m	0.813 m
Bending angle	50°	75°
Gap	100 mm	120 mm
Edge angles	5.8°	29°
Maximum field (500 A)	5.9 kG	8.2 kG

4.1. The magnetic and electrostatic elements

Table 3 summarizes the properties of the magnetic dipoles, which were designed at TRIUMF and manufactured commercially for use in DRAGON. Both magnetic dipoles are equipped with Nuclear Magnetic Resonance (NMR) probes to measure the magnetic field precisely while all of the quadrupoles are equipped with Hall probes.

The electrostatic dipole specifications are given in Table 4. All electrodes were made of titanium

Table 4
Properties of DRAGON electrostatic dipoles

	ED1	ED2
Bending radius	2.00 m	2.5 m
Bending angle	20°	35°
Height of electrodes	280 mm	300 mm
Gap	100 mm	100 mm
Gap uniformity	0.1 mm	0.1 mm
Maximum voltage	±200 kV	±160 kV

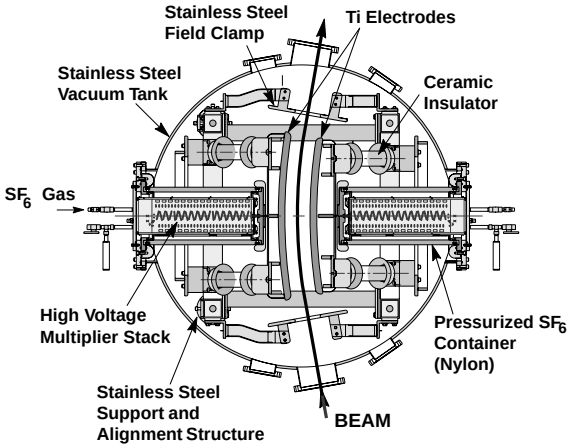

Fig. 9. Schematic view of the electrostatic dipole system.

for best spark resistance to pitting. The support frames allowed precision adjustment of the inter-electrode gap and the adjustment of the gap between field clamps and the electrodes assembly, after which frame, electrodes and field clamps were installed as a unit in the vacuum tank and aligned with respect to the ion-optical axes. Fig. 9 shows the arrangement of electrodes and high-voltage stacks; the latter operate in SF_6 at 2 atm absolute. Sections of 6-mm thick lead sheets were formed to fit, and epoxied externally to the lid, side and underside of the vacuum tanks, to provide protection from X-rays (especially during electrode conditioning).

Magnetic quadrupoles Q1 through Q8 were designed at TRIUMF and manufactured commercially. All except Q2 had pole tips of hyperbolic shape, to minimize non-quadrupole field components over a large fraction of the aperture. The poles of Q2 were shaped to produce a 5% sextupole component at the pole-tip radius. Quadrupoles Q9 and Q10 became available after their use in a TRIUMF collaborative project, and the four sextupoles were originally used in TRIUMF's meson channels. Four x–y steering magnets capable of deflections up to 20 mrad complete the set of electromagnetic elements in the separator.

4.2. EMS vacuum system

The separator vacuum system was designed with a common roughing line and common backing line, each with its own oil-free pump (Leybold Dry-vac). The principal volumes of the system are the two electrostatic dipole (ED) tanks and the three diagnostics boxes located upstream, between, and downstream of the tanks. Each tank is equipped with a 1000 l/s turbomolecular pump (Varian V1000HT) for pumping down to high vacuum, a cryopump for use during operation of the ED, and an ion pump for maintaining high vacuum between periods of operation.

Pressures in the ED tanks are typically $1–2 \times 10^{-8}$ Torr when isolated and $3–4 \times 10^{-7}$ Torr when opened to the adjoining sections of the system. The diagnostics boxes have typical pressures of $1–2 \times 10^{-6}$ Torr.

4.3. Diagnostics and controls

Beam tuning diagnostic devices are grouped at three focus locations. Each set consists of a Faraday cup with bias ring, a pair of horizontally moving slits and a pair of vertically moving slits. Currents as low as 10 pA can presently be read from the Faraday cup or slits. In addition, there are six beam centering monitors (BCM) which consist of four plates whose currents can be combined to show when the beam is centered on the ion-optic axis. The BCM's are positioned such that, when used in combination with the slits and target cell aperture, the beam can be put on-axis at two locations in each of the five straight-line segments of the separator. The BCM's sensitivity

has been more than adequate for tuning radioactive beams at typical ISAC intensities.

A "beta monitor" measures the intensity of radioactive beam stopped on the slits at the end of the first stage of mass separation. It consists of two 6 mm thick plastic scintillators, one behind the other, recording the passage of electrons. The two counters operate in coincidence mode, and are sensitive to electrons having enough energy to pass through the front detector into the back one. Most of the radioactive beams of interest decay by positron emission, with most of the β energy spectrum above the detection threshold. The beta monitor, in conjunction with the beam monitor in the gas target, will provide a check on (1) isotopic composition of the beam and (2) unexpected loss of beam, between the gas target and the mass selection slits.

Fields of the magnetic dipoles are measured with an NMR probe located outside the vacuum vessel but still in the flat-field region. The quadrupoles are equipped with Hall probes, located where the magnetic fields reach a maximum. The quadrupoles were field-mapped, allowing the pole-tip field to be scaled from the Hall probe measurement.

For a control system DRAGON adopted Experimental Physics and Industrial Control System (EPICS), which was already in use for the ISAC accelerator controls [16]. The vacuum components of the gas target and separator have their interlock logic programmed into a programmable logic controller (PLC). A bus system (Canbus) links magnet power supplies, Hall probes, and ED power supplies to the control system. An auxiliary program can carry out scaling of magnet and ED settings as required for ions of a specified mass, charge, and energy. Data may be transferred between EPICS and the online database of the experimenters' data acquisition system.

4.4. EMS Commissioning with ISAC beams

Separator 'tuning' has proven to be relatively straightforward. It is done either with the radioactive beam directly or with a stable 'pilot' beam, requiring current of at least 40 epA (electrical). Quadrupoles and sextupoles are set according to the mass, selected charge state, and nominal energy of the beam after passing through the gas target. The beam energy is then determined by finding the MD1 field which puts the beam on-axis at the charge-selection slits (current sensitive) and using faraday cup FCCH . These slits are closed to 2 mm during this tuning stage. Calibration of NMR readings at well-known capture-resonance energies confirmed the expected relationship, namely,

$$\frac{E}{A} = k\left(\frac{qB}{A}\right)^2 \tag{1}$$

with $k = 48230\ \mathrm{keV}/u/(\mathrm{Tesla}/u)^2$, where E is the kinetic energy of a beam particle, A its mass in atomic mass units (u), q its charge state and B the magnetic field in MD1. Such energy calibration studies are continuing [7]. Timing measurements between various DRAGON detectors and the ISAC RF system used to generate the beam pulse also provide a measure of the beam energy. Further, the delivered beam energy is also checked by the ISAC operators using a dipole magnet system upstream of DRAGON.

Steering magnets are used to center the beam on the BCM device at the entrance of ED1, then ED1 is adjusted to center the beam at the Mass selection slits. Fine-tuning of beam direction through the second stage is continued using MD2, ED2, and steering magnets with BCM 3–6 and the final slits. When beam has been tuned through to the Faraday cup, FCF following the Final slits, the ED voltages are reduced by the ratio of masses of beam and recoil particles, to transmit recoil particles rather than beam.

Commissioning of the separator using stable beams was done in two distinct modes. In the first, the gas target was replaced by a double-steering magnet so that the beam could be deflected horizontally or vertically through angles comparable to the largest cone angle of recoil particles from capture reactions of interest. By varying the initial angle or the beam energy, it was possible to confirm that the desired focus conditions were obtained at the three slit locations and the achromaticity condition was met at the Mass and Final selection slits. Using a deflection of 10 mrad

to simulate the ^{21}Na(p,γ)^{22}Mg reaction at E_{cm} = 212 keV, a transmission of 95±3% through the target to the first Faraday cup was measured with stable beam ^{20}Ne at 200 keV/u [7].

In the second mode of operation, the gas target was in place and resonant proton capture reactions, well-known from studies with non-inverse kinematics, were used. These included resonances of the ^{21}Ne(p,γ)^{22}Na reaction with E_{cm} = 731.5 keV and with E_{cm} = 258.4/259.3 keV, of ^{20}Ne(p,γ)^{21}Na with E_{cm} = 1112.7 keV, and of the ^{24}Mg(p,γ)^{25}Al reaction with E_{cm} = 402.2 and 790.4 keV [17]. The resonances for the radiative proton capture on ^{21}Ne are sufficiently strong that with beams of 1 pnA it was possible to investigate transmission as a function of slit openings, efficiency of the γ array, and related issues in a relatively short period.

5. The DSSSD end detector

Mounted at the end of the 21 m length of the electromagnetic separator is a thin-window, double-sided-silicon-strip detector (DSSSD), Micron Semiconductor Model W(DS)-250. The DSSSD detector has 16 strips of 3 mm pitch, on the front and on the back. Heavy ions traversing the separator produce pulses in a front strip and a back strip to register their 2d-position and energy. Energy spectra acquired from strip detectors have a tail at pulse-heights below the full energy peak, due to inelastic absorption and partial charge collection for events in the gaps between strips [18].

The tail region is important because this is the region of pulse-heights where the very rare capture events will populate the spectra. A much larger number of unseparated (i.e. leaky) beam particles are detected at energies a few percent higher than the recoil ions' energies. A low-energy tail from these "leaky beam" particles will contaminate the region of the recoils to a greater or lesser extent, depending on the intrinsic detector response. However, the part of the leaky beam and its gap events that are in the tail region are not correlated with the γ rays and will be eliminated in coincidence spectra (see Section 9).

5.1. α particle tests of the DSSSD

Between the 3 mm wide strips are gaps of width 110 μm. Ions detected in the gaps may produce a pulse-height in the tail region of the full energy peak. To measure this effect, we collimated an α source (^{241}Am) with a paper slit to produce a beam approximately 180 μm wide. Positioning the slit collimator over one of the gaps between strips on the front surface of the detector produced the pulse-height spectrum shown in Fig. 10c. Fig. 10b displays the spectrum from one strip of an uncollimated α source as a comparison. The fraction of events in the tail region of the spectrum (once background has been subtracted from the spectrum) is proportional to the gap/collimator width ratio, indicating that all of the events in the gap produce a pulse height lower than the full energy peak. Most gap events lie within a peak at about 1/2 the full pulse height, allowing for reliable interpretation of recoil spectra.

Since the detector's thickness is large compared to the range of heavy ions, the back-side strips are relatively far from the site of the charge creation compared to the front strips. Lateral track-spreading degrades the back-side energy resolution, and shifts more events into the low-energy tail compared to the front side. Because the separator's bending elements bend the recoils horizontally the DSSSD was oriented to measure the horizontal position with the front strips.

5.2. Heavy ion beam tests of the DSSSD

DRAGON was tuned to transmit a minuscule beam of 1.0 MeV/u ^{16}O ions with energy and time spread much better than the expected detector's energy and time resolutions. The measured energy and time resolutions were therefore attributed entirely to the intrinsic detector performance. Fig. 10a shows an energy spectrum acquired from a typical front strip with beam and α-source simultaneously present. The "gap events" are concentrated in a peak at approximately 1/2 the full beam energy. The average energy resolution at 1.0 MeV/u was 1.4% FWHM and the time resolution was 1.2 ns, both averaged over the 16 front strips.

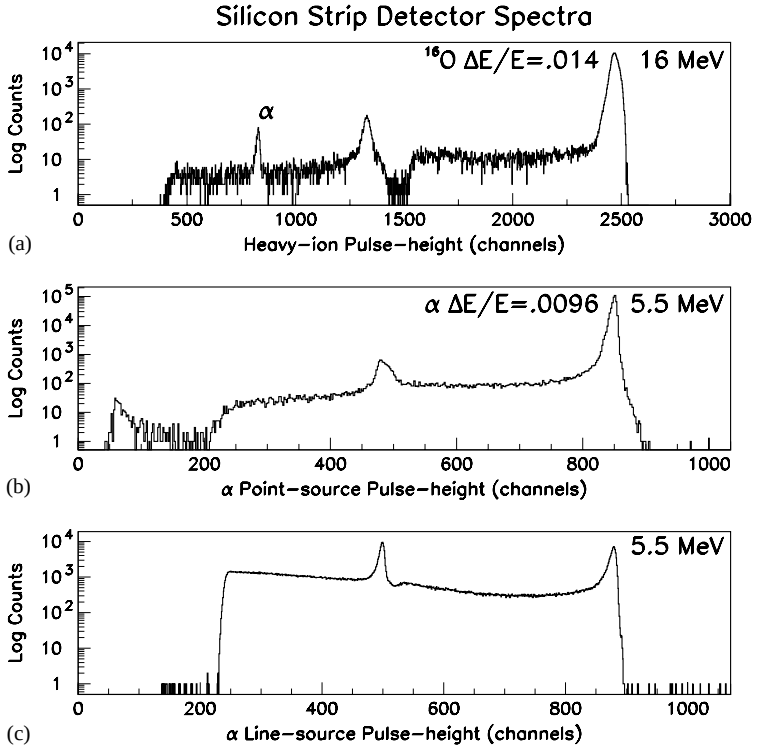

Fig. 10. (a) 16 MeV oxygen beam energy spectrum in one front strip of the DSSSD. Lower energy peaks from gap-events and α source are also present. (b) Spectrum using an ^{241}Am α source uniformly flooding one typical strip. (c) α spectrum of a line source collimated to illuminate mainly the gap between two strips.

6. Elastic-scattering monitor detectors

Fig. 2 shows the gas target enclosure and elastic monitor telescopes. One telescope at 30° and one at 57° share a rectangular front collimator. At the back of each telescope, behind circular collimators, two ORTEC Ultra Cam silicon detectors of area 150 mm^2 are mounted. These are collimated to view a central portion of the intersection line of beam with gas. For a fixed beam geometry, each detector measures an elastic scattering rate proportional to the product of beam current times target gas pressure. Since gas pressure is independently measured by a manometer, the elastic rate is a measure of beam current. The integrated monitor count is the primary measure of the integrated beam current during a run.

Fig. 11a shows a 2d spectrum of pulse-height vs. r.f.-time from the 30° detector and with a 225 keV/u ^{21}Na beam. The span of times on the vertical axis is the period of the r.f. wave, 85 ns. The projection of the 2d spectrum on the horizontal, i.e. energy, axis is shown in Fig. 11c. In this spectrum, the elastic scattering peak rides on an exponential background from the positron decay of the ^{21}Na beam scattered in or near the target. The background extends to higher energies than the elastics. In the time spectrum, shown in Fig. 11b, the elastics ride on a uniform random background, which makes subtraction fairly straightforward.

The elastic detector is also used to monitor the relative beam energy during the course of a run. The beam energy is initially set by the accelerator operators by temporarily diverting the beam into a calibrated magnetic spectrometer upstream of the DRAGON target. Once the data taking starts, the time of flight of the elastic scattering is used to verify that the beam energy stays constant during the many hours of a run. Fig. 11d shows the

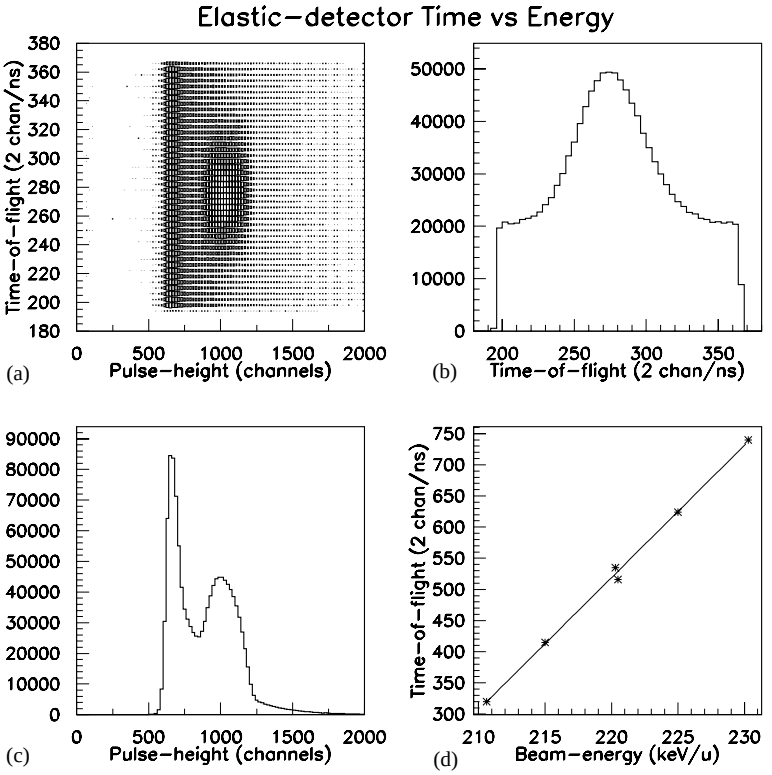

Fig. 11. Elastic monitor spectra using a ^{21}Na beam with $E = 225$ keV/u (see text): (a) 2d pulse-height vs. r.f. time-of-flight, (b) time spectrum projected from the upper panel, (c) pulse-height spectrum projected from the upper panel, and (d) elastic time of flight as a function of beam energy.

relationship between the time measured by the elastic monitor and the beam energy measured (following passage through the gas target) at the energy-dispersive focus following the first magnetic dipole of the EMS, using an NMR probe. The good consistency between time and energy demonstrates that the elastic monitor provides a reliable measure of energy fluctuations, with a precision of about 0.1% at 225 keV/u.

7. Modular electronics and computer interface hardware

The detectors described above are connected to modular electronics housed in 2 NIM, 1 CAMAC, and 1 Eurocrate powered chassis. Fig. 12 shows a block diagram of the electronics with the detectors on the left and the acquisition computer on the right. Separate paths to dedicated buffer memories are provided for the gamma and heavy-ion ADC/TDC (Analogue Digital Converter/Time-Digital Converter) data.

The elastic monitor detector, not shown, is multiplexed to share gate generation electronics and buffer memory with the heavy-ion detector. Elastic and heavy-ion pulses occur asynchronously and at low rates; therefore, multiplexing does not create additional dead time.

Each buffer memory can accommodate up to 16,384 words of data, enough for about 1000 γ or heavy ion events. When a memory becomes 3/4 full, it generates a CAMAC "look-at-me" (LAM) which signals the acquisition computer. The remaining 1/4 capacity of a memory continues to acquire events until the computer responds to the LAM, which allows for random response latency. The computer responds to a LAM from either

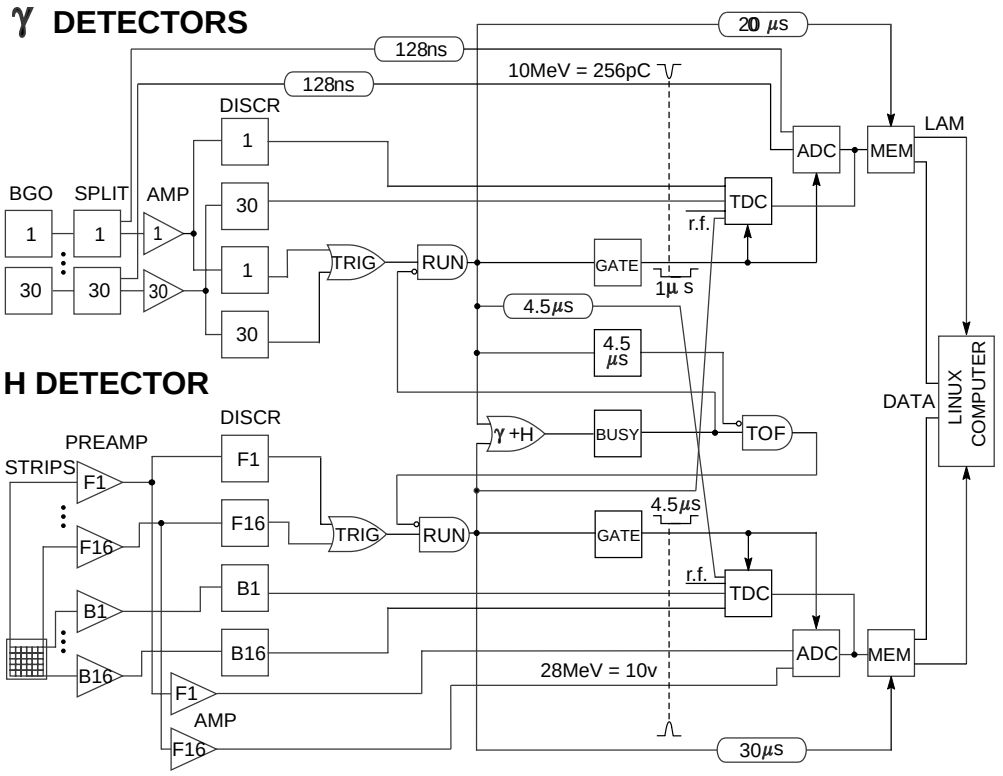

Fig. 12. Block diagram of DRAGON data acquisition electronics. Definition of terms: ADC = Analogue to Digital Converter, AMP = Amplifier, BGO = Bismuth Germinate, DISC = Discriminator, MEM = Memory, TDC = Time to Digital Converter.

memory by reading both memories using a single-crate CAMAC controller module in the crate.

The computer sorts the data into separate γ singles, heavy-ion singles, elastic monitor (singles), and γ/heavy-ion coincidences based on the pattern of each event's TDC/ADC data. Coincidence events are recognized by the occurrence of valid TDC conversions indicating that the γ and heavy-ion records were detected within 1–4 μs, the characteristic time-of-flight of the heavy ion through the 21 m separator.

7.1. γ-detector electronics

The anode outputs from the 30 γ detectors' PMTs are carried by 50-Ω cables to 30 rack-mounted resistive splitters (Fig. 12). One output of each splitter goes to an ADC through a delay-line. The other output is amplified 10X and then sent to a leading-edge-discriminator (LED). A second output from the 10X amplifier feeds a 8 MHz low-pass filter, which in turn feeds a constant-fraction-discriminator (CFD). The 30 CFD outputs are combined in a logical OR to generate a γ master-gate signal. This then generates gates for the ADC's and starts signals for the two 32-channel TDCs. The master-gate also starts a 20 μs busy gate which holds off the occurrence of additional gates until the ADCs and TDCs have finished converting and transfer their data into memory.

The width of the master-gate sets the ADC integration time of the linear signals at the input of charge-sensitive-ADCs. A gate width in the range 100–1000 ns may be selected under computer control. So far only 1000 ns has been used in experiments, though shorter times may be useful in future to reduce the effects of pile-up. The γ

detector's BGO scintillator has a decay constant of 300 ns [11]. For short gate widths, incomplete charge integration omits some of the PMT signal and results in degraded energy resolution due to limited photoelectron number statistics. The selected gate width, 1000 ns, is a compromise between high-rate capability (i.e. short times) and optimum energy resolution (i.e. long times), but favors good energy resolution.

The logical OR of the 30 CFD signals marks the event start-time and imposes the condition that at least one BGO detects a γ-ray with energy exceeding a fairly high energy-threshold ($\approx$2 MeV). After a 128 ns delay during which the master-gate is generated, all 30 ADCs are gated on. At least one, the one containing the trigger pulse, will convert during the gate period. The γ-ray which caused the master-gate may be accompanied by other γ-rays, either from the cascade decay of the recoil nucleus, or secondary γ-rays created by the Compton scattering or pair-production of a primary γ-ray in the BGO. These extra γ-rays are detected and converted by o ther ADCs, with the same master-gate. In general an event may have a complex pattern of ADC pulse-heights which is untangled in the analysis software.

Due to their high rate-handling capability, the leading edge discriminators (LED) provide the most accurate measure of γ-ray times. Each LED output goes to a separate TDC stop. The TDC measures the time of both leading and trailing edges of the LED pulse, so that pulse-width is recorded in addition to leading-edge arrival time. Time slewing of the TDC conversions comes from several sources, some of which can be corrected by software analysis and/or calibration. For example, the slewing from multiple detector triggers in the CFDs is removed by subtracting the RF time from the LED time measured in the same TDC.

The most important slewing comes from the difference in electronic transit times among the 30 PMTs. These transit times were measured using a ^{60}Co source to measure the time differences between pairs of detectors operated in coincidence. These differences were recorded in the computer and thereafter subtracted event-by-event to correct each LED/TDC conversion.

7.2. Heavy ion detection electronics

The electronics for the double-sided-silicon-strip detector (DSSSD) were developed at the Rutherford-Appleton Laboratory [19] and are also used for the TUDA (TRIUMF UK Detector Array) detectors at TRIUMF [20]. In DRAGON, the 32 strips' signals are connected to 32 charge-sensitive, RAL108 preamplifiers (Fig. 12) in an aluminum box bolted to the vacuum box at the end of the separator. The preamplifiers produce shaped, charge-sensitive pulses with 50 μs decay time, suitable for input to a shaping amplifier.

The preamplifier-output signals are carried in a 22 m cable bundle to amplifier and discriminator modules, housed in a Eurocrate near the target. The shielded cable bundle contains differentially driven twisted pairs, one pair from each preamplifier, as well as other individually shielded coaxial cable and twisted pairs, e.g. preamplifier test-pulses and DC power for preamplifiers.

Each of 32 RAL109 amplifier/discriminators produces a 0–10 V shaped linear signal and a leading-edge discriminator logic pulse. The discriminator levels are manually adjustable in groups of 8, via front-panel pots on the amplifier/discriminator modules. The 16 linear signals from the front strips are connected to individual 4000-channel ADCs.

A logical OR of the 16 discriminator outputs from the front strips forms the heavy-ion trigger. The output of the gate generator triggers on a peak-sensing ADC for each strip. This also starts a 32-channel TDC, which receives the 16 back discriminator signals as 16 stop inputs. Measuring the time between front and back strips' discriminators, provides the possibility of analyzing pulse shape, but this feature has not been used in analysis.

In addition to the 16 channels from the back strips, the heavy ion's TDC receives a stop from the γ array's master-gate, delayed by a CAMAC-controlled delay-generator. The selected gate delay-time is presently set to 4.5 μs, slightly longer than the longest heavy ion flight time expected in experiments. This delay setting guarantees that the TDC will have a valid conversion for γ coincidence

events, even for the slowest of heavy ions. The presence of a valid conversion in the relevant TDC marks a heavy ion as being accompanied by a γ-ray in the previous 4.5 μs. On the other hand, the absence of this TDC conversion marks the heavy ion as a singles event. Thus the pattern of heavy ion TDC data provides the information needed to distinguish coincidence events from singles events in the analysis.

7.3. Elastic monitor electronics

The elastic monitor detector is connected to a Canberra 2003B preamplifier, which is followed by an ORTEC delay line amplifier, and by a Tennelec TC451 constant fraction timing single channel analyzer (CF-TSCA). The output of the CF-TSCA generates a trigger for the elastic ADC/TDCs through a common gate generator with the heavy ion, as described above. The delayed output of the ORTEC amplifier is converted in an ADC, separate from but identical to the ones used for the heavy ion. The elastic monitor events therefore occur in the same memory list as the heavy ions. They are distinguishable by their ADC address and sorted into separate spectra by the analysis software.

8. Data acquisition software

The Midas standard data acquisition system [21] controls the data acquisition while the CERN package paw++ [22] displays the online spectra. The essential functions of data acquisition are performed by the following parallel processes running on a PC under Redhat Linux operating system: (1) CAMAC setup and CAMAC data reading by "Frontend"; (2) event-by-event data and scalers' writing to disk by "Logger"; (3) histogram formation and data monitoring by "Analyzer"; (4) histogram display and analysis by "paw++"; and (5) setup parameter storage and process control by "ODBEdit". ODBEdit is a command-line-interpreter which manages input-to and output-from an on-line data base (ODB) stored in shared memory.

8.1. The "Frontend" software functions

Frontend is a program controlled by "start" and "stop" commands. In response to "start", CAMAC is made ready for the first event, by copying selected portions of the ODB to selected registers in CAMAC modules. Once ready, Frontend wakes up whenever a LAM occurs and periodically in response to the computer's clock. In response to a LAM, Frontend reads the CAMAC memories and sends event-by-event data to Logger and Analyzer programs. Periodically Frontend reads all the CAMAC scalers, clears them, and sends their current values to Logger and Analyzer. In response to "stop", Frontend inhibits further data acquisition by generating a veto level through a CAMAC output register.

LAM's occur when either the γ or heavy-ion memories become 3/4 full (see earlier discussion). Three types of events are constructed by Frontend and sent to Logger and Analyzer. Gamma and heavy-ion singles are sent as exact images of the memory contents at the time that the LAM is serviced. However, not every LAM results in a memory transfer. A software prescaler from the ODB reduces the volume of singles data by a selectable integer factor. Different prescaler factors for γ and heavy-ion detectors reflect the large difference in rates between γ detections and heavy-ion detections. With prescaling, comparable statistics are chosen to be obtained for the two types of singles data. Each LAM from the heavy-ion memory forces a read of the γ memory, ensuring that all coincidence data are recorded.

In the LAM service routine, coincidence events are recognized among the more numerous singles events by searching memory contents to find appropriate heavy-ion TDC data. A coincidence event is assembled in the computer's memory by copying the associated portions of the CAMAC memories into a coincidence data region separate from the singles data regions. The NIM/CAMAC hardware provides redundant measures of heavy-ion time-of-flight in both γ-TDC and heavy-ion-TDC. Coincidence events are recorded independently of what prescale factors are chosen. Maximum event acquisition rate is limited to 10,000 events/s by the CAMAC

memory transfer speed and the TDC conversion times.

8.2. The "Analyzer" software functions

The Analyzer program is called once for each processed event. One part calibrates and converts the event-by-event data from CAMAC to internal-format, and one part increments histograms in a common region of memory. Histograms in memory are in the format used by the CERN standard "physics analysis workstation", paw++ [22] software package, which runs in parallel with Analyzer.

The conditions for incrementing each histogram are displayed as a hexadecimal value of a 32-bit mask word, user-defined for each histogram. The values of the bits of the mask word specify logical tests which must satisfy an "AND" condition on a given event to update the appropriate histogram. The conditions are single-channel-analyzers defined by lower and upper limits on the event parameters.

9. Preliminary analysis of radiative proton capture

The first radioactive beam time available into the DRAGON facility was used to study a reaction of astrophysical interest, namely the resonant radiative proton capture of ^{21}Na to form states in ^{22}Mg [23]. This preliminary and partial analysis is presented here only for the purpose of extracting the suppression factor to validate the proper operation of the facility, and for the planning of future measurements. Two resonances were investigated in detail, a narrow resonance at $E_{cm} = 212$ keV [23], and a broad resonance at $E_{cm} = 863$ keV [20,23].

The beam energy was scanned in 5 keV/u steps over the laboratory energy of the narrow resonance, 210–230 keV/u. A thick-target yield curve, similar to the one shown in Fig. 7, was obtained. Three energies on the flat portion of the yield, where the narrow resonance is contained in the target, were summed to produce the histograms shown in Fig. 13. Fig. 13a shows the singles energy spectrum in the end detector. The peak is at the

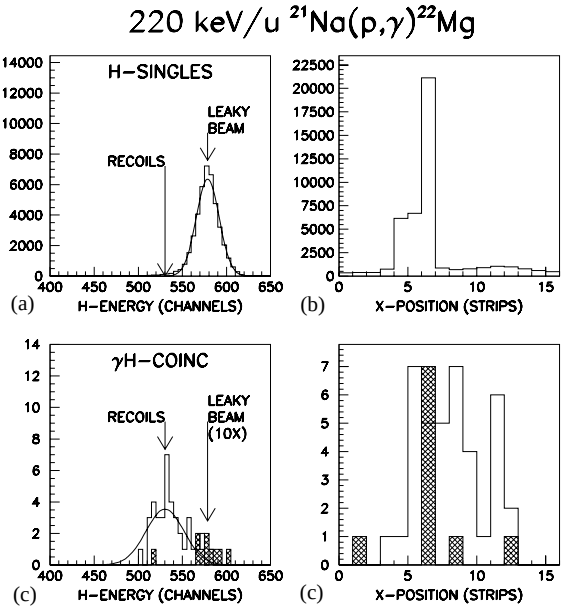

Fig. 13. Typical histograms, summed over three beam energies, from off-line analysis of the ^{21}Na(p,γ)^{22}Mg $E_{cm} = 212$ keV resonance: (a) end detector singles-mode energy spectrum showing leaky beam peak, (b) end detector singles-mode horizontal-position spectrum, (c) end detector coincidence-mode energy spectrum showing recoils peak, and (d) end detector coincidence-mode position spectrum. Cross-hatched events are from a displaced time window, i.e. random events.

energy of the beam, which "leaks" through the separator as described in Section 4.4. Fig. 13c shows the same spectrum but imposing the γ-ray coincidence requirement. The vertical scale of Fig. 13c is about 1000 times smaller than Fig. 13a, showing the essential role that the γ coincidence plays in separating the recoils' signal from leaky beam background. The distribution of the singles and coincidence events in horizontal (x) position at the end detector are displayed in Figs. 13b and d, respectively. The recoils are well contained inside the 5×5 cm^2 detector, which was previously shown to have uniform efficiency in its central region [12].

The remaining background with the coincidence requirement is shown as the dotted histogram marked "Leaky beam" in Fig. 13c. These four events are random coincidences between leaky beam and positron background in the γ array, obtained from an off-time window in the

coincidence time spectrum. For this resonance, the random background can be estimated through a combination of energy windows (in the γ spectrum) and subtraction. However, for weaker resonances the random events will grow to outnumber the reals, and subtraction will no longer work.

For narrow resonances of known energy, such as this one, it may not be the best use of beam time to scan the energy over the resonance. It is possible to validate that the beam energy is on a narrow resonance even with a single measurement. Fig. 14 shows the spectrum of counts as a function of γ detector position, for the same three beam energies shown in Fig. 13. The position of emission of γ-rays is localized along the beam line. The "Mean" values of the three spectra, shown in Fig. 14, allows the determination of the average position of the resonance with some accuracy. As the energy rises, the mean position of detection marches down the beam line because the higher the beam energy the further into the target it penetrates before reaching the resonant energy. Fig. 14d shows

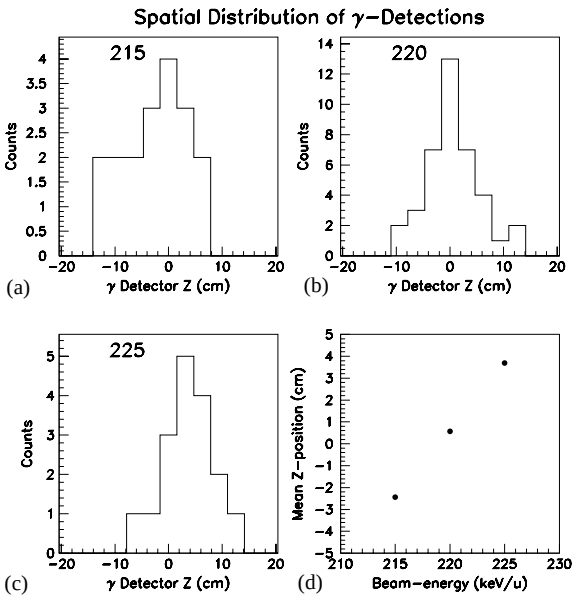

Fig. 14. The number of counts vs. γ-ray detection position along the beam line (see text). As the beam energy rises, the "Mean" detection position moves downstream through the target.

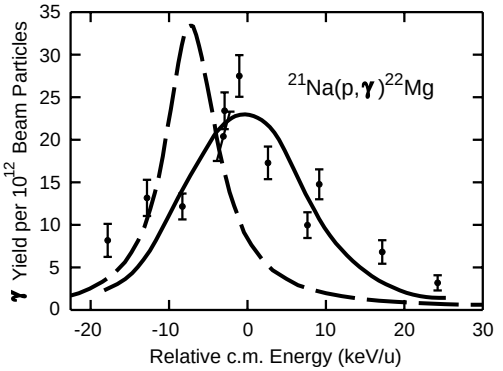

Fig. 15. Excitation function of the resonance at 863 keV/u in the ^{21}Na(p,γ)^{22}Mg reaction. The Breit–Wigner cross section (dashed curve), broadened and shifted by target thickness (solid line) is compared to the data.

several mean Z positions as a function of beam energy.

A broad resonance at 863 keV/u beam energy was scanned in 5 keV/u steps. The proton-width of this resonance [20] is comparable to the calculated gas target thickness of 13 keV/u [6]. Fig. 15 shows the observed yield as a function of center-of-mass energy. To account for the resonance width, the Breit–Wigner cross section, given by the dashed curve, was convolved with the target thickness and beam energy resolution, and fitted to the data to give the solid curve. The feature of such broad resonance scans which differs from narrow resonance scans (cf. Fig. 7), is that the yield varies continuously with beam energy and peaks at the energy which positions the maximum of the Breit–Wigner shape at the approximate center of the target. The strength of the resonance, given by the area under the solid curve, can be determined by the best fit condition.

A key part of the use of DRAGON to determine accurately the resonance strengths of radiative capture reactions, is to measure such values for well studied reactions involving stable beams. Such a series of studies are in progress [7].

9.1. The DRAGON suppression factor

The ability of the facility to measure weak resonances has been quantified by computing the

suppression factor, defined to be

$$S = \frac{N_l}{N_b e} \quad (2)$$

where N_l is the number of leaky beam particles, N_b is the number of incident beam particles, and e is the efficiency of the detectors (including γ efficiency only if the coincidence mode is used). The proposed experiments for DRAGON have been categorized by the suppression factors, shown in the last column of Table 1, required to obtain a one-to-one signal-to-background ratio in the analyzed data e.g. Fig. 13. The suppression factor from the separator varies from 10^{-11} at 850 keV/u to 10^{-9} at 220 keV/u. Energy, timing and position measurements from the recoil detector have given additional suppression factors of 2 to >10, depending on beam energy. Runs at $E_{cm} =$ 212 keV were taken with recoils focussed on the DSSSD rather than the Final slits, which were opened to the full detector size. The data of Fig. 13a, without γ coincidence, gives a suppression factor of 10^{-9} with the EMS only. Including the γ coincidence (Fig. 13c), the suppression factor improves to 10^{-13}, good enough to do most of the measurements initially proposed for DRAGON.

Table 1 shows that the resonance of interest in the $^{15}O(\alpha,\gamma)^{19}Ne$ reaction requires a suppression factor of 10^{-15}, about 100 times better than the suppression factor measured for the $E_{cm} =$ 212 keV resonance in the $^{21}Na(p,\gamma)^{22}Mg$ reaction. However the actual improvement required to attempt the ^{15}O measurement is more than 100X, because the ^{15}O reaction utilizes a lower energy beam, 150 keV/u, and produces a lower energy γ-ray, 4 MeV. Possible improvements in the performance of DRAGON can be made to take us from the present 10^{-13} at 212 keV/u to the desired 10^{-15} at 150 keV/u. Studies in progress indicate that slit settings can be optimized to improve beam suppression ten-fold while maintaining efficient transmission. Insertion of an additional detection system at the focal plane, to measure a local time-of-flight of the ions at the end of the EMS is under development should provide an additional factor of suppression. Using the r.f. time of the γ detection to cut some of the background will also provide an additional factor.

Perhaps the largest improvement factor may arise with the use of new focal plane, gas ionization chamber which may provide elemental selectivity between the beam (O) and recoil (Ne). This has been tested at energies near 500 keV/u but requires study below this energy. The combination of all of these factors resulting from optimizing the performance of DRAGON may provide the necessary beam suppression to perform all of the measurements of astrophysical reaction rates presently proposed (Table 1).

Acknowledgements

The assistance of many groups at TRIUMF in the design, construction and installation of many parts of DRAGON is gratefully acknowledged. The authors thank Bob Laxdal, Matteo Pasini and the ISAC Operators for delivering the ISAC beams used in the commissioning. We acknowledge the contribution of Gordon Ball, Nick Bateman, George Clark, Don Dale, Cary Davids, Uli Giesen, Heinz Biegenzein, Peter Jackson, Rolf Keitel, Peter Lipnik, Peter Machule, Bruce Milton, Miguel Olivo, Doug Preddy, Alan Shotter, Glen Stinson and Hermann Wollnik for many contributions on the design and installation. Thanks to Dennis Healey for design of the gas target recirculation system, to Herb Coombes for design of the PMT bases and γ signal filters, to Peter Gumplinger for configuring the GEANT software used for simulations, and to Pierre-Andre Amaudruz for providing a skeleton Midas DAQ and frequent consultations on acquisition software.

The financial support received from the Natural Science and Engineering Research Council of Canada and from TRIUMF is also gratefully acknowledged. Author U.G. was supported by a Department of Energy grant (DE-FG03-93ER40789). Author S.E. wishes to acknowledge support from the Deutsche Forschungsgemeinschaft (DFG GR 1577-301). Support by a U.S. DOE Grant No. DE-FG02-91ER-40609 is also acknowledged.

References

[1] W. Liu, et al., Charge state studies of low energy heavy ions passing through hydrogen and helium gas, Nucl. Instr. and Meth. A, in press.

[2] D. Gigliotti, A. Hussein, J. Rogers, Calibration and simulation of a gamma array for DRAGON at ISAC, in: J.M. D'Auria, J. Thomson (Eds.), EMIS-14 Conference Proceedings, 2002, Victoria, Canada, 2002, in press.

[3] D. Gigliotti, M.Sc. Thesis, University of Northern British Columbia, in preparation.

[4] W. Liu, M.Sc. Thesis, Department of Chemistry, Simon Fraser University, 2001.

[5] C. Rolfs, W. Rodney, Nucl. Phys. A 235 (1974) 450.

[6] James Ziegler, SRIM—Stopping and Range of Ions in Matter, http://www.srim.org/.

[7] Sabine Engel for the DRAGON Collaboration, Commissioning and operation of DRAGON: results so far, in: J. D'Auria, J. Thomson (Eds.), EMIS-14 Conference Proceedings, 2002, Victoria, Canada, 2002, Nucl. Instr. and Meth., in press.

[8] L. Bonnet, M. Frederic, P. Leleux, I. Licot, P. Lipnik, Nucl. Instr. and Meth. A 292 (1990) 243.

[9] T. Ludziejewski, K. Moszynska, M. Moszynski, D. Wolski, W. Klamra, L.O. Norlin, E. Devitain, V. Kozlov, IEEE Trans. NS-42 (1995) 394.

[10] J.G. Rogers, C.J. Batty, IEEE Trans. NS-47 (2000) 438.

[11] O.H. Nestor, C.Y. Huang, IEEE Trans. NS-22 (1975) 68.

[12] D. Hutcheon, D. Hunter, et al., The Optics of DRAGON TRIUMF Design Note, in preparation.

[13] H. Wollnik, J. Brezina, M. Berz, Nucl. Instr. and Meth. A 258 (1987) 408.

[14] R. Brun, F. Bruyant, A.C. McPherson, M. Maire, P. Zanarine, CERN Data Handling Division, DD/EE/84-1, 1987, Also, GEANT—Detector Description and Simulation Tool, CERN Program Library Long Write-Up W5013, IT Division, API group, CERN.

[15] S.B. Kowalsky, H.A. Enge, Nucl. Instr. and Meth. A 258 (1987) 407;
RAYTRACE is a public domain, TRIUMF-maintained program, Documentation can be found at www.triumf.ca.

[16] R. Keitel, D. Bishop, D. Dale, H. Hui, S. Kadantsev, M. Leross, R. Nussbaumer, J. Richards, E. Tikhomolov, G. Waters, Status Update on the ISAC Control System, ICALEPCS01, San Jose, CA, 2001.

[17] P.M. Endt, Nucl. Phys. A 633 (1998) 1 and references therein.

[18] C. Wrede, A. Hussein, J. Rogers, J.M. D'Auria, A double sided strip detector as an end detector for DRAGON, in: J. D'Auria, J. Thomson (Eds.), EMIS-14 Conference Proceedings, 2002, Victoria, Canada, 2002, Nucl. Instr. and Meth., in press.

[19] P.J. Sellin, P.J. Woods, D. Branford, T. Davinson, N.J. Davis, D.G. Ireland, K. Livingston, R.D. Page, A.C. Shotter, S. Hofmann, R.A. Hunt, A.N. James, M.A.C. Hotchkis, M.A. Freer, S.L. Thomas, Nucl. Instr. and Meth. A 311 (1992) 217.

[20] C. Ruiz, L. Buchmann, T. Davinson, R.E. Azuma, A.A. Chen, B.R. Fulton, D. Groombridge, L. Ling, A. Murphy, J. Pearson, I. Roberts, A. Robinson, A.C. Shotter, P. Walden, P.J. Woods, Phys. Rev. C 65 (2002) 042801(R).

[21] Midas is maintained by Stefan Ritt (http://midas.psi.ch) and Pierre-Andre Amaudruz (http://midas.triumf.ca).

[22] CERN Physics Analysis Workstation users manual is available via internet at http://wwwinfo.cern.ch/asd/paw/.

[23] N. Bateman, K. Abe, G. Ball, L. Buchmann, J. Chow, J.M. D'Auria, Y. Fuchi, C. Iliadis, H. Ishiyama, K.P. Jackson, S. Karataglidis, S. Kato, S. Kubono, K. Kurokawa, X. Liu, S. Michimasa, P. Strasser, M.H. Tanaka, Phys. Rev. C 63 (2001) 035803.